metals

MDPI

Article

Structure, Phase Composition, and Mechanical Properties of ZK51A Alloy with AlN Nanoparticles after Heat Treatment

Anastasia A. Akhmadieva *, Anton P. Khrustalev, Mikhail V. Grigoriev, Ilya A. Zhukov and Alexander B. Vorozhtsov

Faculty of Physics and Engineering, National Research Tomsk State University, 36 Lenin Ave, 634050 Tomsk, Russia; tofik0014@gmail.ru (A.P.K.); mvgrigoriev@yandex.ru (M.V.G.); gofra930@gmail.com (I.A.Z.); abv1953@mail.ru (A.B.V.)

* Correspondence: nas99.9@yandex.ru

Abstract: The paper studies the influence of the content of aluminum nitride nanoparticles on the structure and mechanical properties of the ZK51A magnesium alloy. The microstructure investigations with optical and electron microscopy show that 1 wt.% AlN promotes the best grain refinement and size distribution. According to tensile strength testing of the ZK51A alloy, grain refinement is not a dominating mechanism in the property improvement of the alloy after heat treatment. The maximum values of mechanical parameters are achieved at the lowest (0.1 wt.%) content of aluminum nitride. The main mechanism of mechanical characteristics increase with the addition of AlN nanoparticles is dispersion hardening.

Keywords: magnesium alloys; ZK51A; nanoparticles; aluminum nitride

Citation: Akhmadieva, A.A.; Khrustalev, A.P.; Grigoriev, M.V.; Zhukov, I.A.; Vorozhtsov, A.B. Structure, Phase Composition, and Mechanical Properties of ZK51A Alloy with AlN Nanoparticles after Heat Treatment. *Metals* **2024**, *14*, 71. https://doi.org/10.3390/met14010071

Academic Editor: Ruizhi Wu

Received: 7 October 2023
Revised: 25 December 2023
Accepted: 26 December 2023
Published: 8 January 2024

1. Introduction

Magnesium alloys are considered to be new-generation materials for the space, aviation, and automobile industries due to their processing and operating parameters, low density, machinability, and specific strength [1–3]. Their significant shortcomings include low formability, insufficient mechanical strength, and corrosion resistance. The creation of cast magnesium alloys with improved strength properties can extend the range of their application [4,5].

The Mg–Zn–Zr system alloy ZK51A is one of the promising magnesium casting alloys. The main hardening mechanism of this alloy is a solid solution associated with the solubility of alloying components (Zn, Zr, Cd) in magnesium [6,7]. The presence of zirconium in this alloy provides its fine-grained structure, as this element is one of the most efficient grain refiners in aluminum-free magnesium alloys [8,9]. This is conditioned by the hexagonal close-packed (HCP) structure of both zirconium and magnesium, and zirconium particles act as magnesium nuclei, which generate the additional solidification centers and limit the grain growth during curing, and thus melt in liquid magnesium [10,11].

The structure of the casting alloy is a solid solution of zinc (Z) and zirconium (Zr) in magnesium (Mg). The MgZn intermetallic phase is located along Mg grain boundaries. After heat treatment, the MgZn phase and Zr-based solid solution sediment form the oversaturated solid solution, thereby hardening it [12,13]. In works [14–17], heat treatment of the ZK51A alloy is performed in the mode T1 (300 °C annealing for 6 h followed by cooling in air).

There are methods of increasing mechanical properties of Mg alloys by dispersion hardening with refractory nano- and microparticles [18–21]. In [22–24], aluminum nitride (AlN) is used as a promising compound for hardening Mg alloys, since it has the HCP crystal lattice with a = 0.312 nm and c = 0.4988 nm parameters almost similar to those of the Mg matrix, i.e., a = 0.3209 nm and c = 0.5211 nm [25,26]. AlN nanoparticles used as reinforcing particles are very interesting due to the high specific strength and low

coefficient of thermal expansion, high melting point, and hardness [27,28]. Also, due to the small addition of particles, the cost value of alloys grows insignificantly. Research in this field shows that the incorporation of nonmetal microparticles [23,24,29] and nanoparticles [21,22,30] in the Mg matrix improves its strength properties and refines its grain structure. At the same time, very little published information is available concerning the integrated effect of heat treatment and nanoparticle content in the Mg matrix, including alloys of the Mg–Zn–Zr system. Casting is the most common production method of Mg alloys due to the potentiality of creating diverse shapes, high performance, large-lot production, and high-quality surface of the obtained products [31,32].

However, the use of nanoparticles in the production of casting alloys is associated with problems of agglomeration and flotation, which result in the high porosity of alloys. These problems can be avoided via the introduction of nanoparticles consisting of the master alloy during mechanical [33], ultrasonic [34], and vibration [35] treatment of the melt. Despite a large number of studies showing the positive effect of aluminum nitride nanoparticles on the structure and properties of magnesium alloys, the effect of their content in the metal matrix has still not been sufficiently studied.

The aim of this work is to investigate the effect of heat treatment and dispersion hardening on the ZK51A magnesium alloy with different contents of AlN nanoparticles (from 0.1 to 1 wt.%) on its structure, physical and mechanical properties, and fracture.

2. Materials and Methods

2.1. Casting Magnesium Alloys

Magnesium alloy ZK51A consisting of 93.58 to 95.4% Mg, 4 to 5% Zn and 0.6 to 1.1% Zr produced by a conductor electric explosion in nitrogen [36] and machine-milled magnesium powder MPF-4 were used as initial materials. The AlN nanopowder was preliminary deagglomerated and cleaned ultrasonically in ethyl alcohol for 10 min using an Ultrasonic Cleaner DK-300S. The mass ratio of the AlN nanopowder and ethyl alcohol was 1:5. The micropowder MPF-4 was added to the obtained slurry in the amount of 95 wt.% relative to the AlN content and then ultrasonically treated for 10 min with simultaneous stirring in an ULAB US-2200A overhead stirrer rotating at 160 rpm for 10 min. The powder mix Mg–5 wt.% AlN was dried in a vacuum oven at 70 °C. The obtained powder mix was compressed into tablets using a hydraulic press capable of applying a 4 t load with a steel mold with a working area of 40 mm (Figure 1).

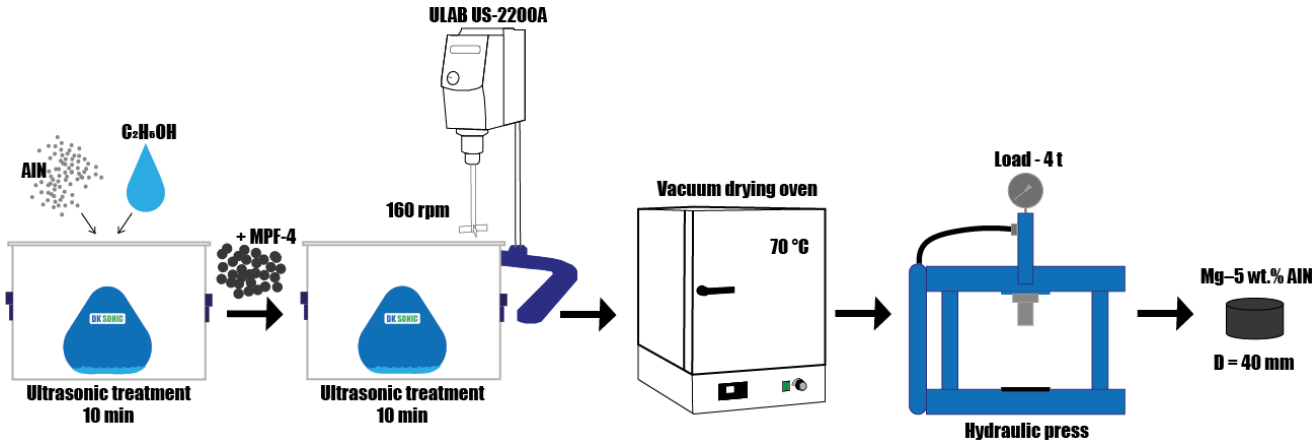

Figure 1. Scheme of obtaining the master alloy.

A total of 2000 g of the ZK51A alloy was placed in the original steel crucible [37] and heated up to 700 °C at a constant argon blow. Then, the melt was mixed for 30 s and introduced in the Mg–AlN master alloy at 690 °C and mixed again at 500 rpm for 1 min. The AlN nanoparticle content in the melt was 0.1, 0.5, and 1 wt.%. At 660 °C, the melt was poured into the steel crucible with a diameter of 35 mm and a height of 200 mm and

subjected to vibrations at 0.5 mm amplitude and 60 Hz frequency until complete melt solidification. The initial ZK51A alloy was fabricated with the same parameters without the introduction of the master alloy Mg–5 wt.% AlN. Heat treatment in the mode T1 was performed in a muffle oven at 170 °C, ageing for 22 h followed by furnace cooling (Figure 2).

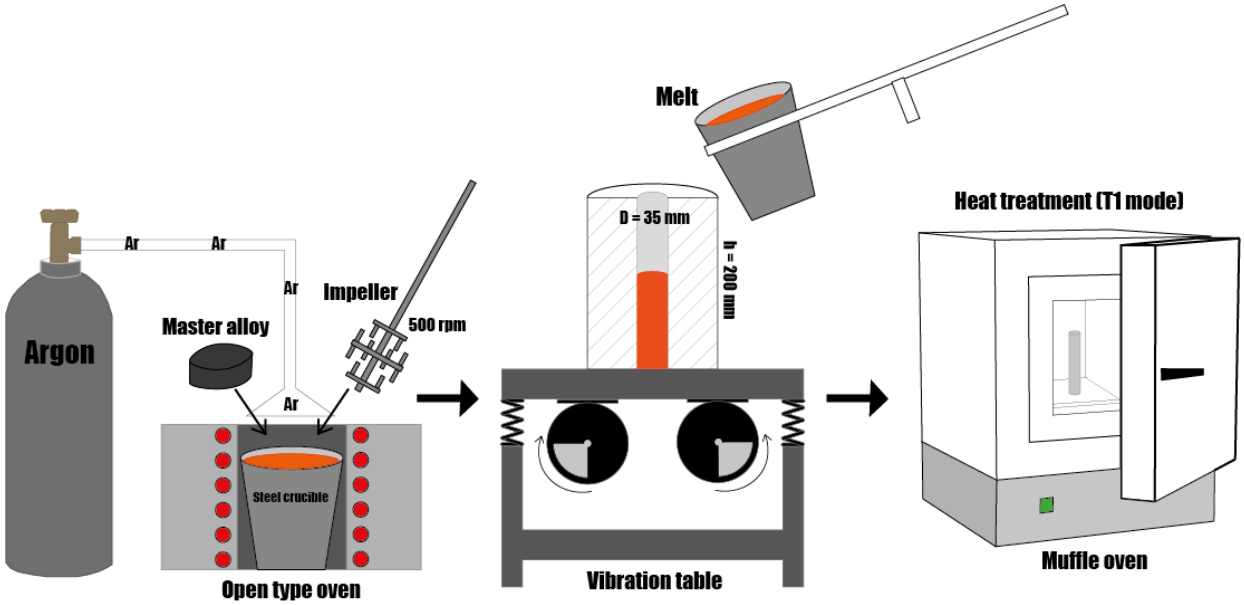

Figure 2. Schematic drawing of the process of the production of alloys.

2.2. Characterization

Initial AlN nanoparticles were investigated on a PHILIPS CM30 Scanning Transmission Electron Microscope (TEM) (Koninklijke Philips N.V., Amsterdam, The Netherlands) using a tungsten cathode. MIRA 3 LMU (Tescan Orsay Holding, Brno, Czech Republic) scanning electron microscope and Olympus GX71 inverted metallurgical microscope (Olympus Scientific Solutions Americas, Waltham, MA, USA) were used to investigate the fine structure of the obtained materials. The alloy surface was etched in picric acid ($C_6H_2(NO_2)_3OH$). X-ray diffraction patterns were recorded on a Shimadzu XRD-6000 Diffractometer (Shimadzu, Kyoto, Japan). Uniaxial tension tests were carried out on 25 × 6 × 2 mm plate-like specimens at a strain rate of 0.001 s^{-1} at room temperature using an Instron 3369 Dual Column Tabletop Testing System (London, UK). Brinell and Vickers hardness testers, Metolab 701 and Metolab 503 (Moscow, Russia), were used to determine the hardness and microhardness, respectively. To measure Brinell hardness, a spherical indenter with a radius of 2.5 mm was used with a force of 62.5 kg and an exposure time of 30 s; the size of the indentations was controlled in the range of 0.2 D < d < 0.6 D. Microhardness testing was carried out on a Metolab 502 microhardness tester using the Vickers method with an indenter in the form of a diamond pyramid (base angle 136°) with a load on the indenter of 50 g and a dwell time of 20 s.

3. Results and Discussion

Figure 3a presents the TEM image of AlN nanoparticles obtained by the conductor electric explosion. The average particle size is 83 nm (Figure 3b). The powder also consists of 200 μm particle agglomerates. The elemental composition of this powder is presented in Table 1.

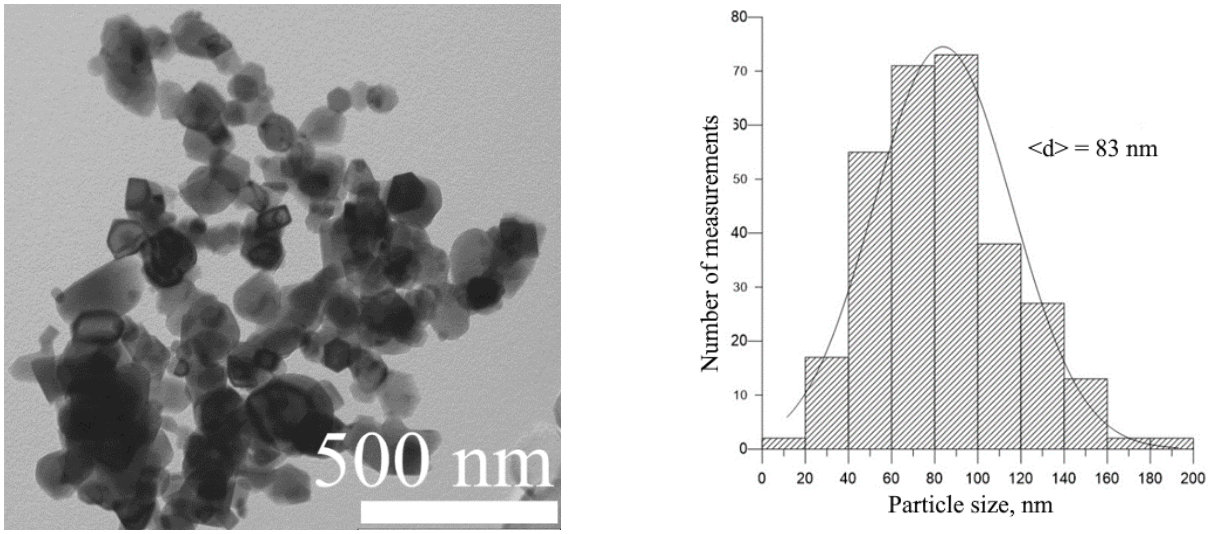

(**a**) (**b**)

Figure 3. A TEM image of the AlN powder (**a**) and a block diagram of the particle distribution (**b**), where <d> is the average particle size.

Table 1. Elemental composition of AlN powder, wt.%.

Al	N	Si	C	S	Fe	O	Cl	Cu	Ni	P
66.8621	31.6132	0.1524	0.0561	0.0013	0.0354	1.1026	0.1178	0.0217	0.0192	0.0182

According to the X-ray diffraction (XRD) analysis, the initial ZK51A alloy consists of α-Mg with lattice parameters a = 0.32040 nm and c = 0.52005 nm, which correlates with the data from [38,39]. The phase composition analysis of the alloy specimens with nanoparticles shows the presence of aluminum nitride with the content varying in a wide range that can be attributed to the nonuniform particle distribution and a small scan area. The size of the coherent scattering region (CSR) of the AlN phase is within the range of the measured powder particle size. Heat treatment does not affect the SCR size of AlN nanoparticles, although for the solid solution Mg–Zn, it significantly grows. Figure 4 and Table 2 show parameters of phases and the structure of synthesized alloys.

In Figure 5a–d, the optical images demonstrate the ZK51A–AlN alloy microstructure at the center of the sample after etching using a polarizing filter. The average grain size of the initial alloy (Figure 5a) is 46 μm, while at the center and edge of the ingot, it is 69 and 35 μm, respectively, which is associated with the rapid cooling near the wall of the chill mold. In the case of 0.1 wt.% AlN (Figure 5b), the grain boundaries are well-defined, the average grain size is 53 μm, and grains become larger towards the ingot center. In the case of 0.5 (Figure 5c) and 1 wt.% AlN (Figure 5d), the structure is homogeneous, with the average grain size of 46 and 54 μm, respectively. The grain refinement is probably conditioned by the formation of additional solidification centers due to the incorporation of AlN nanoparticles uniformly distributed throughout the melt [23].

Optical images in Figure 6 show the ZK51A alloy microstructure after polishing before etching, before and after heat treatment, and after the addition of AlN nanoparticles. The microstructure without nanoparticles has dark elongated inclusions distributed in the ingot volume, which are probably intermetallic compounds of the Mg–Zn system located at the grain boundaries [17,40]. Spherical inclusions in the grain body are identified as the Zn–Zr phase.

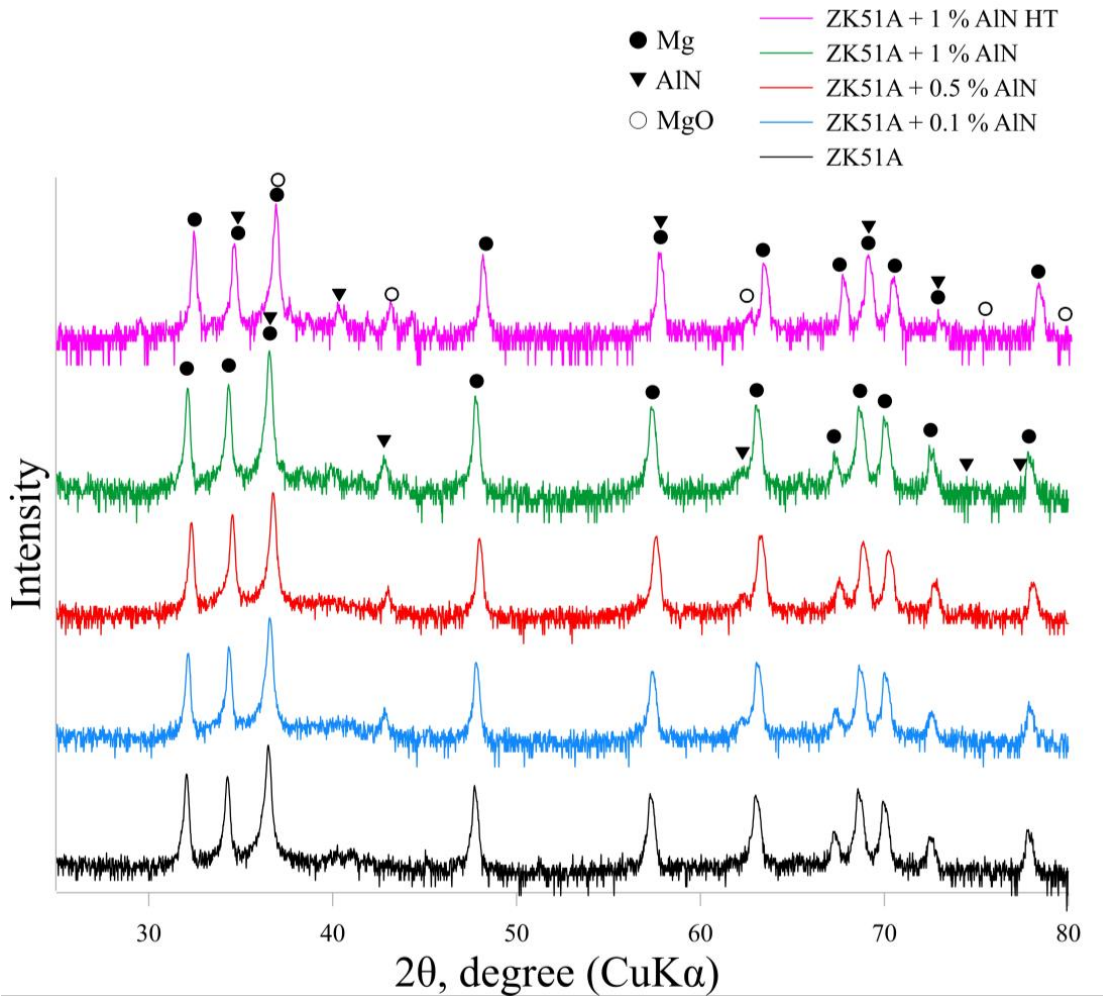

Figure 4. XRD patterns of synthesized alloys.

Table 2. Parameters of phases and the structure of synthesized alloys.

Alloy Specimens	Phases	Phase Content, wt.%	Lattice Parameters, Å	CSR Size, nm	Δd/d·10^{-3}
ZK51A	α-Mg	100	a = 3.2040 c = 5.2005	57	0.8
ZK51A + 0.1 wt.% AlN	α-Mg	88	a = 3.2038 c = 5.2006	65	0.2
	AlN	12	a = 4.2324	39	1.1
ZK51A + 0.5 wt.% AlN	α-Mg	97	a = 3.2028 c = 5.1977	83	1.4
	AlN	3	a = 4.2018	10	4.8
ZK51A + 1 wt.% AlN	α-Mg	95	a = 3.2058 c = 5.2046	84	0.8
	AlN	5	a = 4.2634	27	0.8
ZK51A + 1 wt.% AlN (HT)	α-Mg	97	a = 3.2048 c = 5.2091	319	1.3
	AlN	2	a = 4.5003	45	1.9

The MgZn intermetallic content of the initial alloy after heat treatment considerably grows and is located nearby the ingot edges. After the addition of AlN nanoparticles, a lot of defects appear in the structure, and the MgZn and ZnZr phases remain. The MgZn intermetallic creates 'filaments' linking to each other. The alloy structure consisting of 1% of nanoparticles, is characterized by darker grain-style inclusions throughout the ingot before and after heat treatment. Perhaps, either etching during polishing, or a large number of nanoparticles result in the formation of the new phase. After heat treatment, the microstructure does not significantly change with the nanoparticle addition.

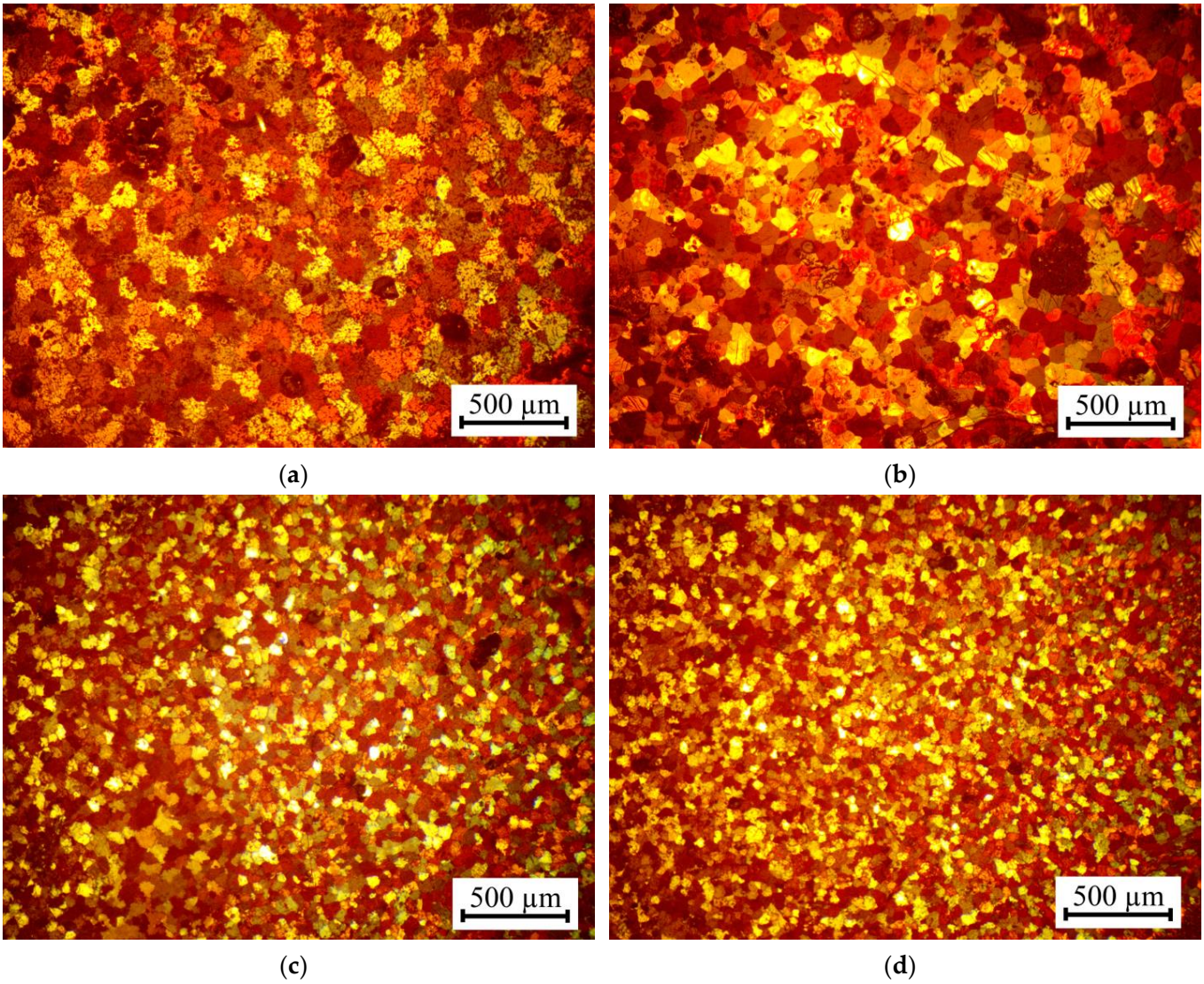

Figure 5. Optical images of the alloy microstructure with different AlN content: (**a**) ZK51A, (**b**) ZK51A + 0.1 wt.% AlN, (**c**) ZK51A + 0.5 wt.% AlN, and (**d**) ZK51A + 1 wt.% AlN.

SEM images in Figure 7 demonstrate the alloy microstructure with 1% of AlN nanoparticles before and after heat treatment. One can see that the microstructure does not differ in either states of the alloy. It consists of equiaxial grains with the average size of 54 µm. The MgZn intermetallic in the Mg–Zn–Zr system alloy appears along the grain boundaries and serves as a grain-growth constraint [13,16]. The ZnZr phase inclusions are not found as, in theory, they appear in the grain body. The cross-sectional analysis does not show inclusions on the surface. The dark areas in the SEM images represent pores formed due to imperfect casting technology.

SEM in combination with energy dispersive X-ray spectroscopy (SEM-EDS) in Figure 8, shows large dark areas identified as fragments of the Mg–AlN master alloy. In addition to the MgZn phase, the intergranular space consists of the Zr-containing phase. According to [9,16], the Mg–Zn–Zr system cast alloys consist of 4.5 to 8.5% of zinc and 0.8 to 1.0% of zirconium, and the latter generates Zn_2Zr_3, $ZnZr_2$, and Zn_2Zr phases. Depending on the heat treatment conditions, the region with ZnZr intermetallic formations can change. Figure 9 presents the elemental composition of inclusions in the ZK51A + 1% AlN alloy after heat treatment. Heat treatment promotes homogenization of the alloy microstructure

due to diffusion interaction between the elements of the undissolved master alloy and the magnesium matrix.

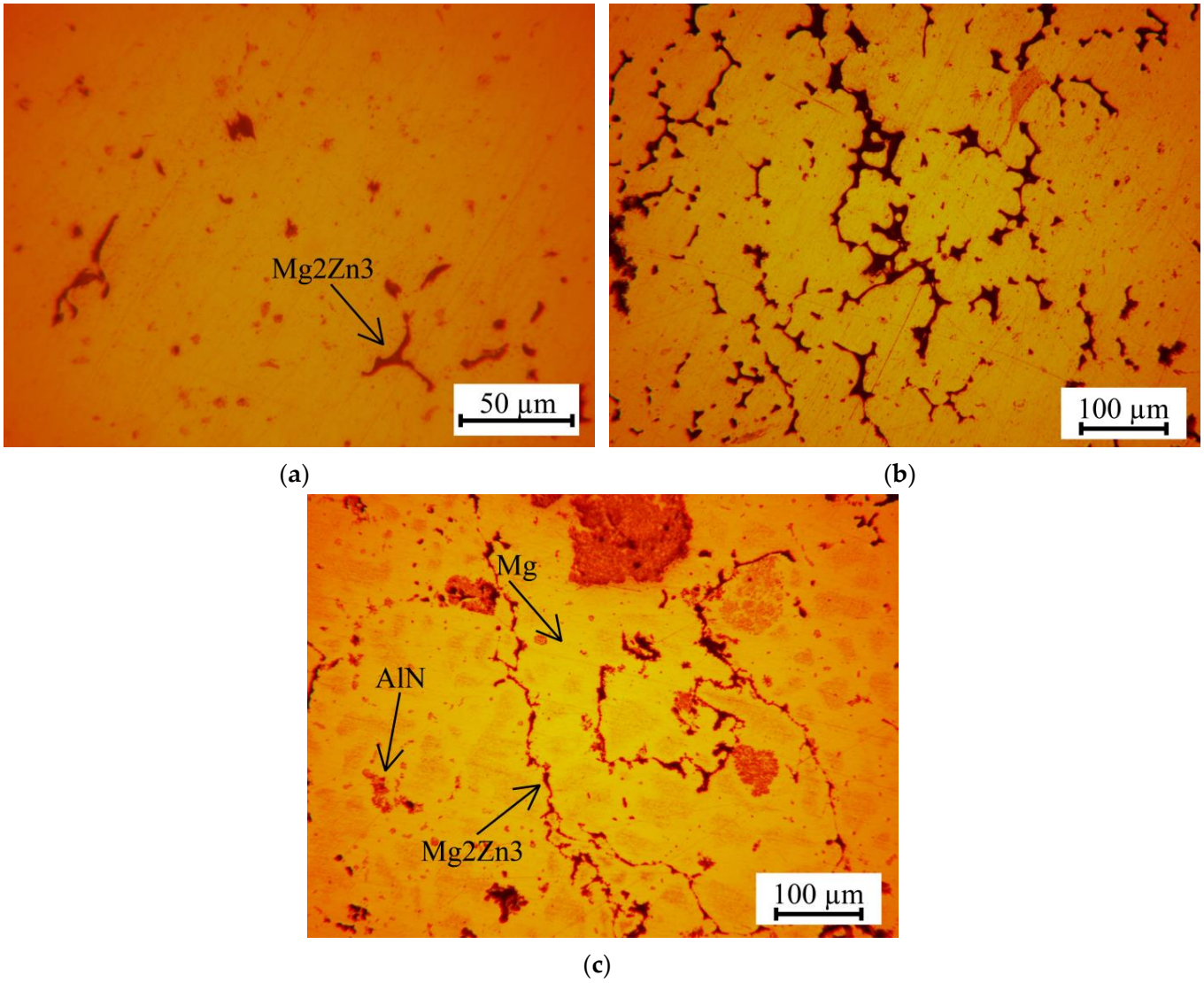

Figure 6. ZK51A alloy microstructure: (**a**)—without AlN nanoparticles, (**b**)—after heat treatment in mode T1, and (**c**)—with 1 wt.% AlN before heat treatment.

Table 3 summarizes measurement results of the hardness and density of the alloys obtained. Figure 10 contains plots of the grain size and hardness relative to the AlN content in cast alloys and alloys after heat treatment. One can see that the hardness lowers from 55 to 47 HB with the nanoparticle content increasing from 0.1 to 1 wt.%, regardless of heat treatment.

Dependence of the grain size and porosity of the AlN content in cast and heat-treated alloys are presented in Figure 11. The average porosity does not exceed 2.5%, while its lowest value (0.5%) is gained after the addition of 0.1 wt.% AlN. When the AlN content increases up to 0.5 and 1 wt.%, the porosity reaches 1.3 and 2.5%, respectively. This can be attributed to additional gases penetrating in the melt during the nanoparticle introduction.

The microhardness AlN content dependence on the AlN content are given in Figure 12 for the alloy before and after heat treatment. It is found that heat treatment has no effect on the microhardness, while the increased nanoparticle content results in its reduction, i.e., 62 and ~50 HV for the initial alloy and the alloy with 1 wt.% AlN, respectively.

Table 3. Parameters of ZK51A–AlN cast alloys and alloys after heat treatment.

Alloys	Hardness, HB	Density, g/cm^3	Grain Size, μm
ZK51A	56 ± 2	1.79 ± 0.1	46 ± 26
ZK51A (HT)	59 ± 1	1.79 ± 0.1	
ZK51A + 0.1 wt.% AlN	54 ± 3	1.8 ± 0.1	53 ± 29
ZK51A + 0.1 wt.% AlN (HT)	55 ± 1	1.8 ± 0.1	
ZK51A + 0.5 wt.% AlN	51 ± 2	1.8 ± 0.1	46 ± 18
ZK51A + 0.5 wt.% AlN (HT)	52 ± 2	1.79 ± 0.1	
ZK51A + 1 wt.% AlN	44 ± 4	1.78 ± 0.1	54 ± 17
ZK51A + 1 wt.% AlN (HT)	50 ± 3	1.77 ± 0.1	

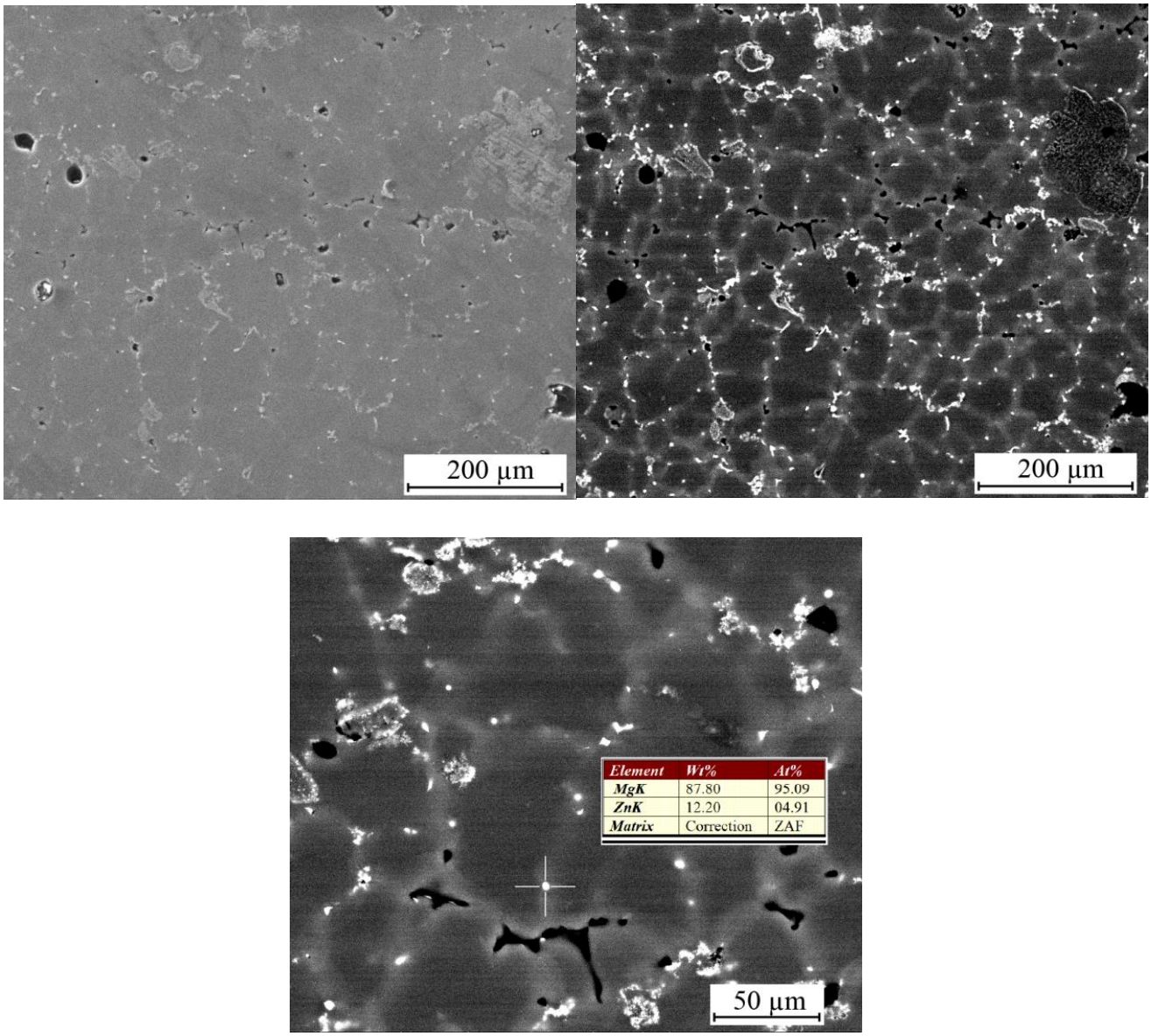

(**a**)

Figure 7. *Cont.*

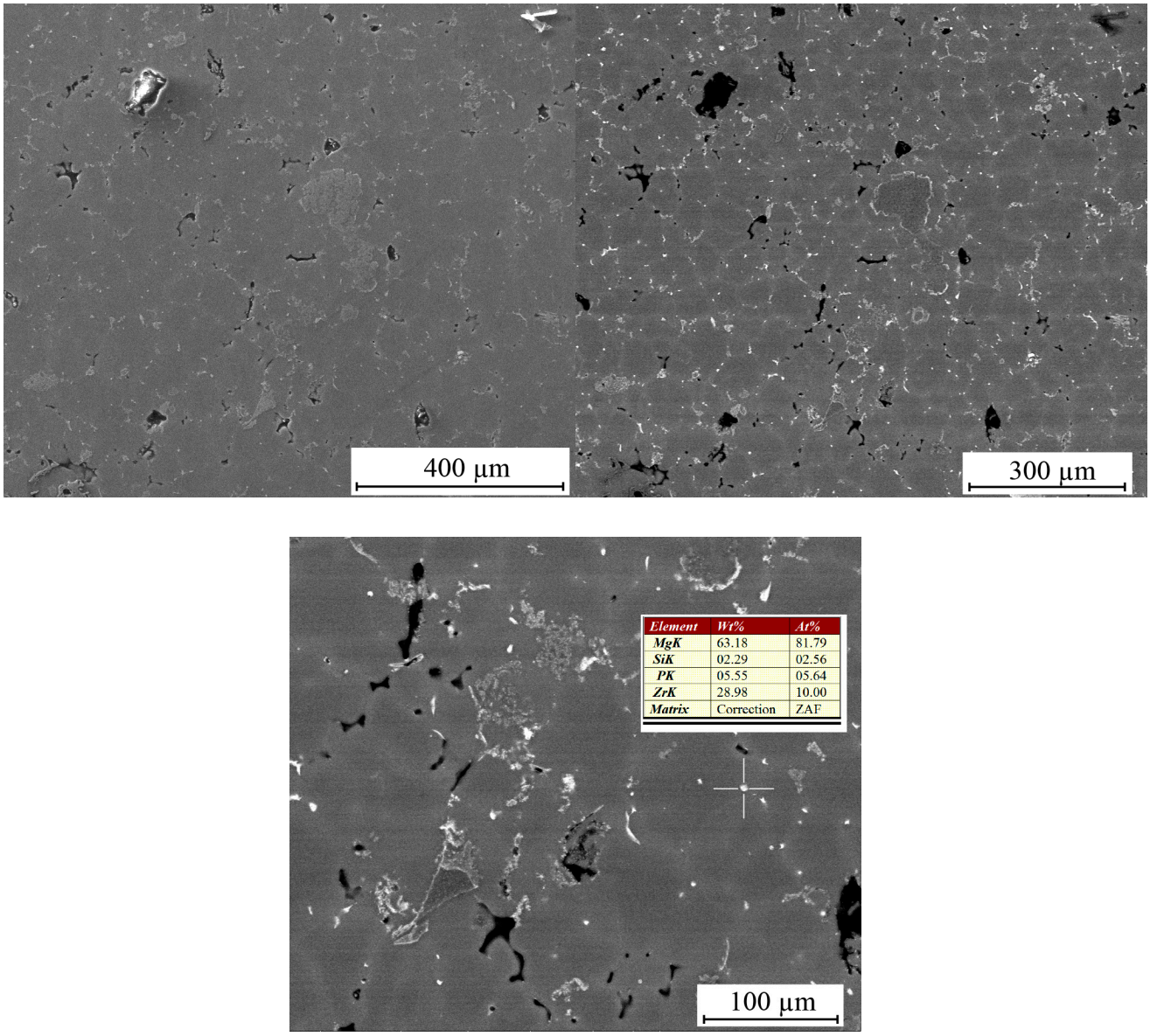

Figure 7. SEM images of ZK51A + 1% AlN alloy structure before (**a**) and after (**b**) heat treatment. White crosses indicate the area of elemental analysis.

Figure 13 presents the stress–strain curves for the obtained alloys after heat treatment. As can be seen from Table 4, the yield strength, tensile strength, and plasticity of the initial alloy without nanoparticles are 63 MPa, 151 MPa, and 6.4%, respectively. After the addition of 0.1, 0.5, and 1 wt.% AlN nanoparticles, the yield strength grows up to 72, 67, and 86 MPa, respectively. The highest growth in the yield strength and plasticity relative to the initial allo, is observed at 0.1 wt.% AlN, viz. from 151 to 212 MPa and from 6.4 to 19.7%, respectively.

The main mechanism of the mechanical characteristics increase with the addition of AlN nanoparticles is dispersion hardening. It is suggested that the introduction of particles into the alloy structure can lead to the deflection of a potential crack from the grain boundary into its volume, as well as greater involvement of the metal matrix in the deformation and fracture process [41,42]. These results are in agreement with earlier studies on the introduction of AlN particles into the AZ91 alloy [37]. However, this effect

is achieved by adding particles in an amount not exceeding 0.1 wt.%. As the number of particles increases, agglomerates are formed, which do not maximize mechanical properties and result in additional fracture centers.

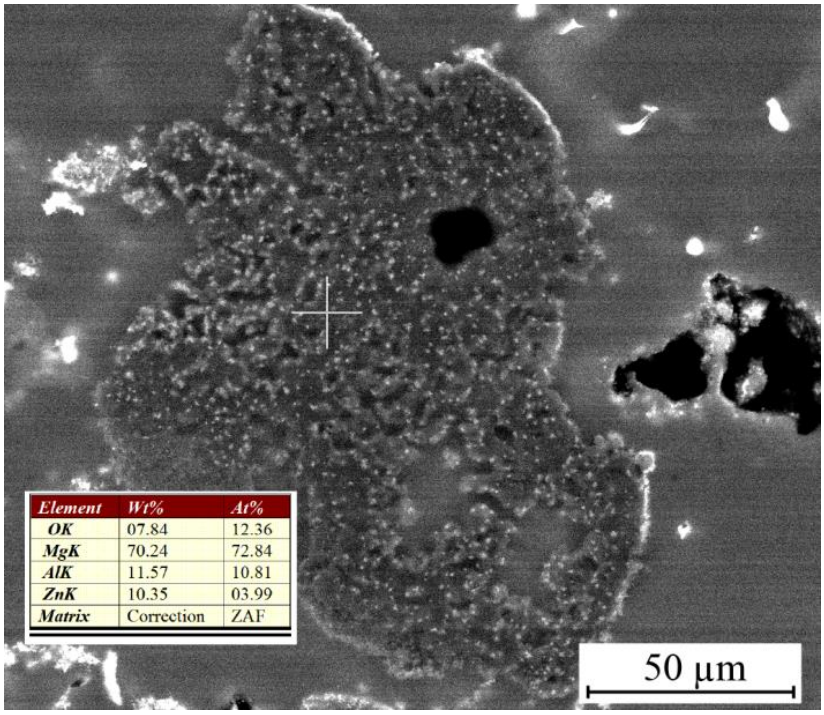

Figure 8. SEM-EDS of master alloy fragments in ZK51A + 1% AlN alloy before heat treatment. A white cross indicates an elemental analysis area.

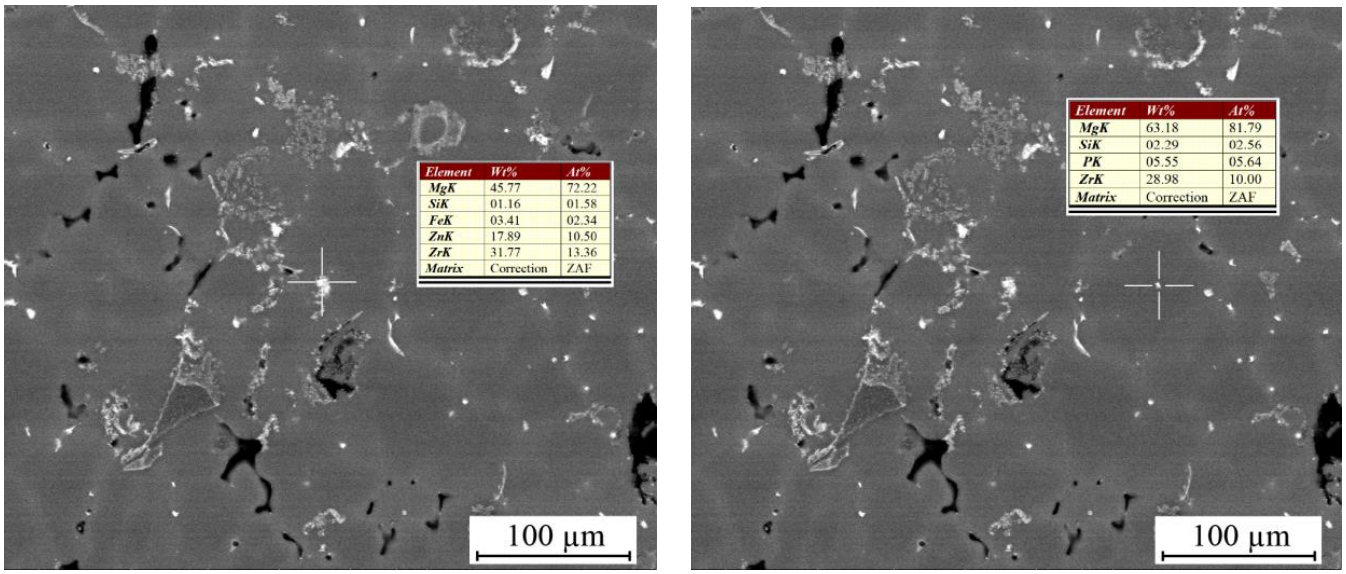

Figure 9. Elemental composition of inclusions in the ZK51A + 1% AlN alloy after heat treatment. White crosses indicate the area of elemental analysis.

The increase in yield strength values of the alloy occurs in accordance with the Hall-Petch law, according to which $\sigma_{0.2}$ increases when a uniform fine-grained structure is achieved [43].

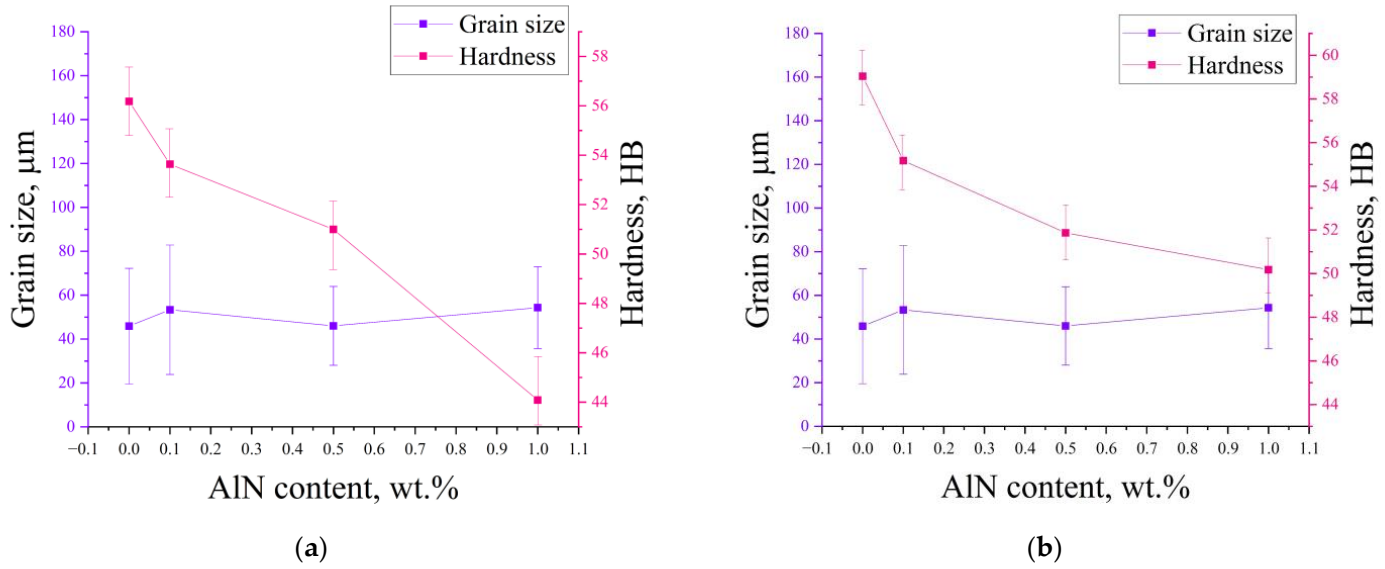

Figure 10. Dependence of grain size and hardness of AlN content in cast (**a**) and heat-treated (**b**) alloys.

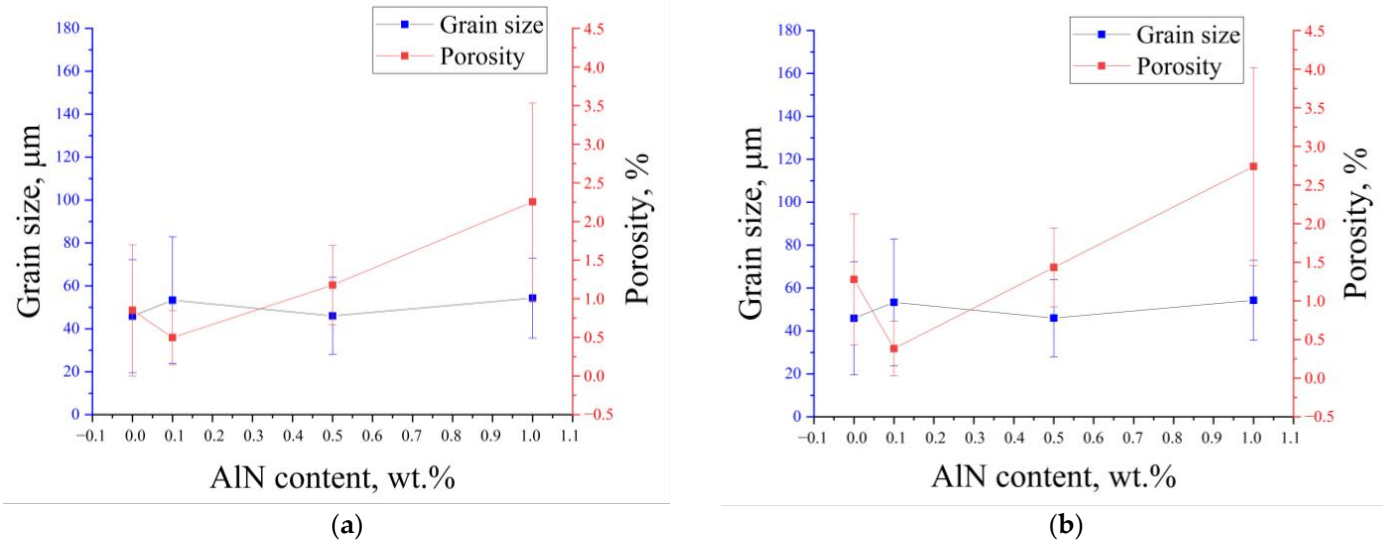

Figure 11. Dependence of grain size and porosity on AlN content in cast (**a**) and heat-treated (**b**) alloys.

SEM observations of the fracture surface after tensile strength testing show a ductile transgranular fracture mechanism for all alloys. SEM images of the fracture surface of heat-treated alloys are presented in Figure 14a–d. There is a particle coalescence comprising aluminum (see Figure 15). These results would suggest that although introduced non-uniformly, AlN nanoparticles are present in the structure and thus some of them cannot be identified due to their nanoscale size.

Using magnification in Figure 16, we identified ~5 μm inclusions on the fracture surface of heat-treated ZK51A + 1 wt.% AlN alloy, which consisted of zirconium. Supposedly, these inclusions were the ZnZr phase, which, in theory, released inside the grain in the form of coarse particles [16].

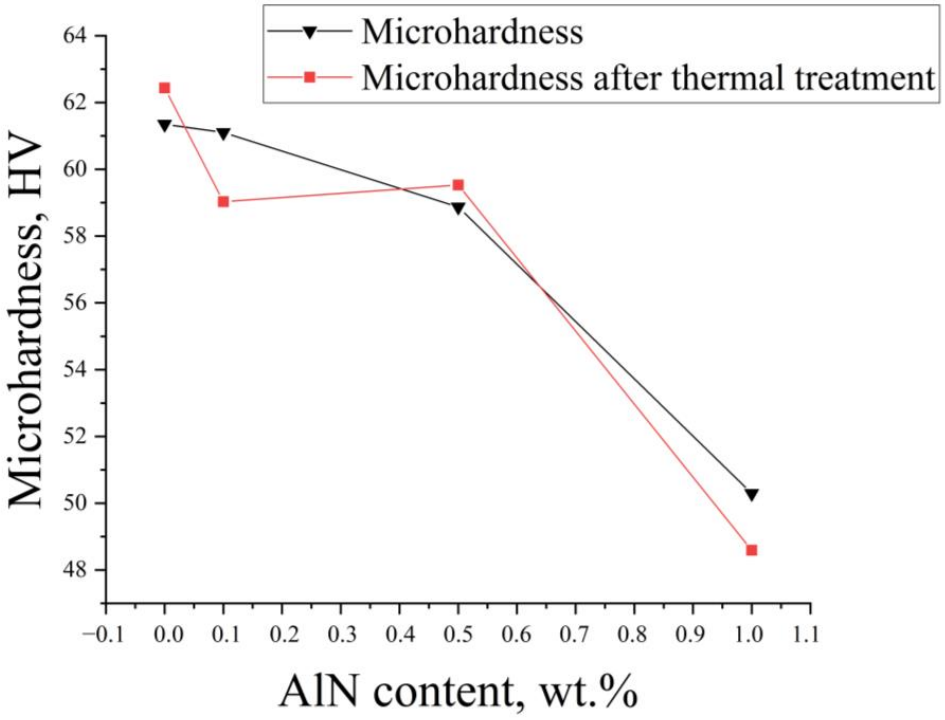

Figure 12. Microhardness dependence on AlN content before and after heat treatment.

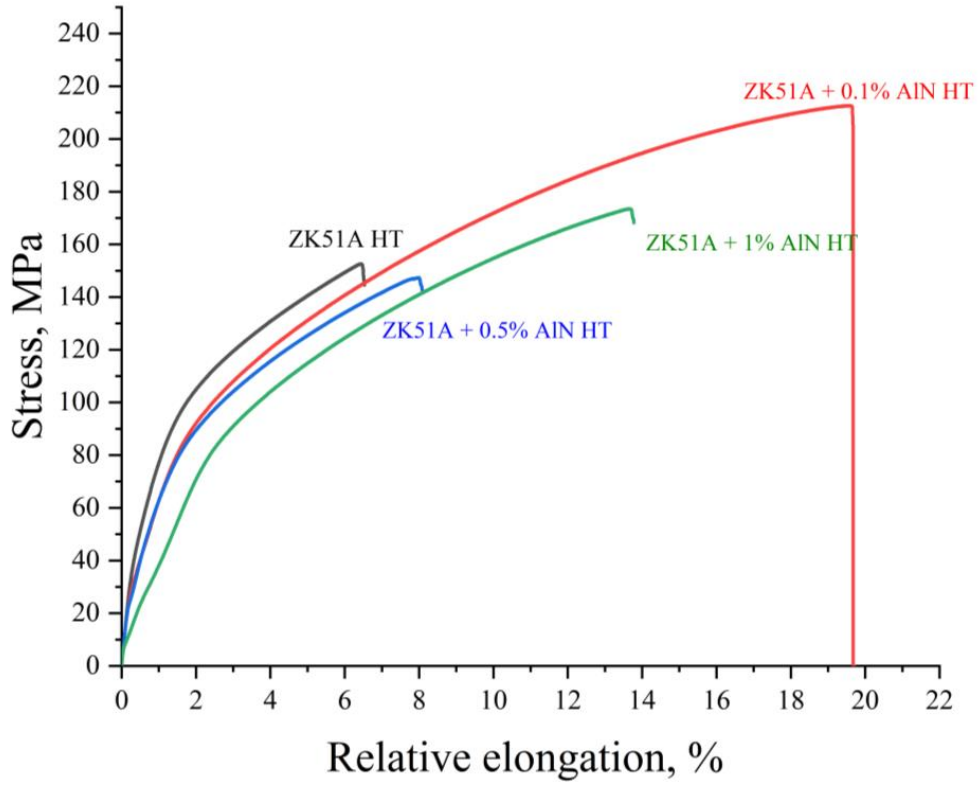

Figure 13. Stress–strain curves of alloys after heat treatment.

Table 4. Mechanical properties of ZK51A–AlN cast alloys and alloys after heat treatment.

Alloys	$\sigma_{0.2}$, MPa	σ, MPa	ε, %	Microhardness, HV
ZK51A (HT)	63 ± 4	151 ± 8	6.4 ± 0.4	62.5 ± 9.2
ZK51A + 0.1 wt.% AlN (HT)	72 ± 7	212 ± 11	19.7 ± 0.6	59 ± 9.6
ZK51A + 0.5 wt.% AlN (HT)	67 ± 5	148 ± 5	8 ± 0.7	59.5 ± 9.4
ZK51A + 1 wt.% AlN (HT)	86 ± 5	174 ± 6	13.8 ± 0.3	48.6 ± 6.1

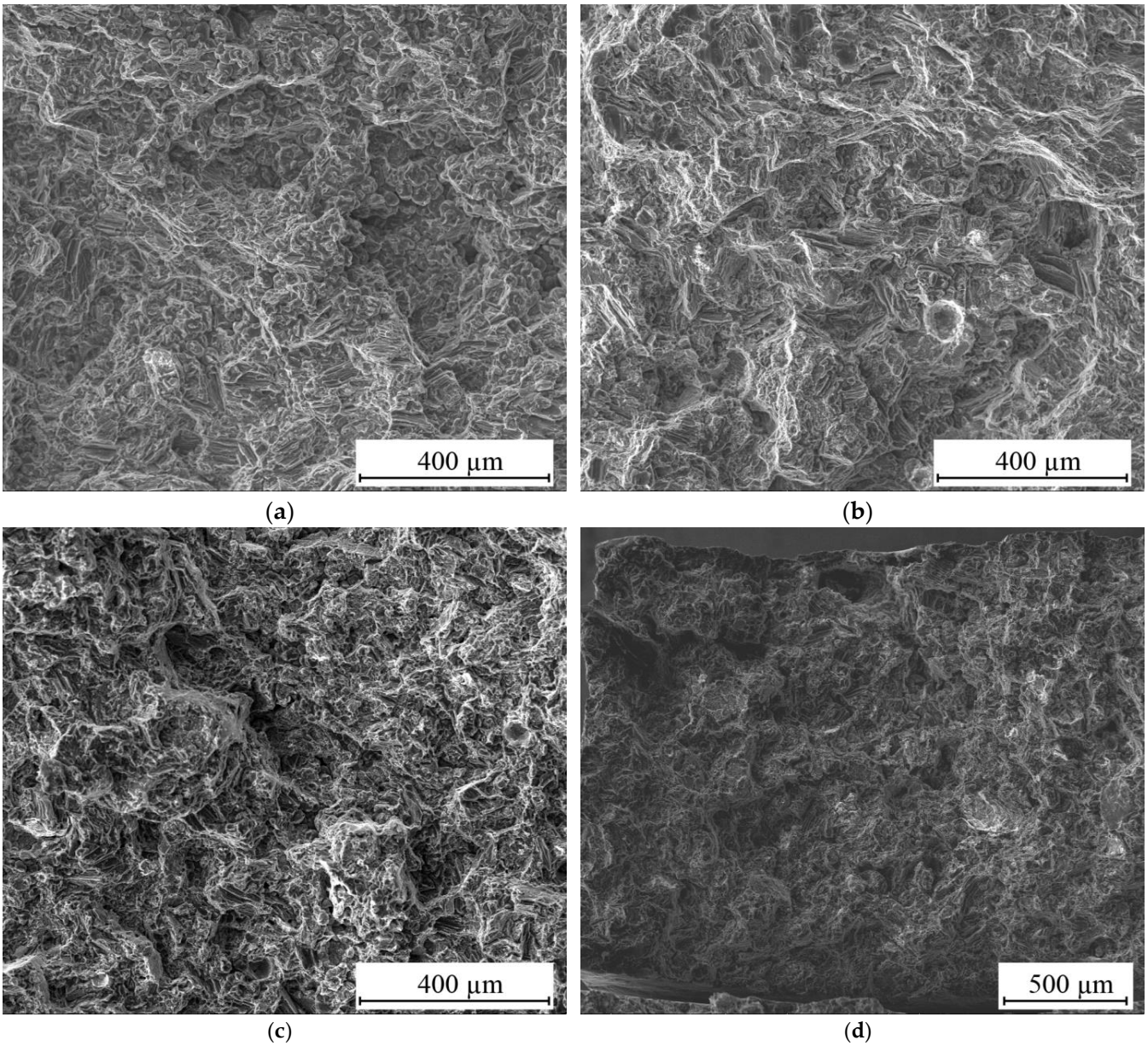

(**a**) (**b**) (**c**) (**d**)

Figure 14. SEM images of the ductile fracture surface of heat-treated alloys failed after tensile strength testing: (**a**) ZK51A, (**b**) ZK51A + 0.1 wt.% AlN, (**c**) ZK51A + 0.5 wt.% AlN, and (**d**) ZK51A + 1 wt.% AlN.

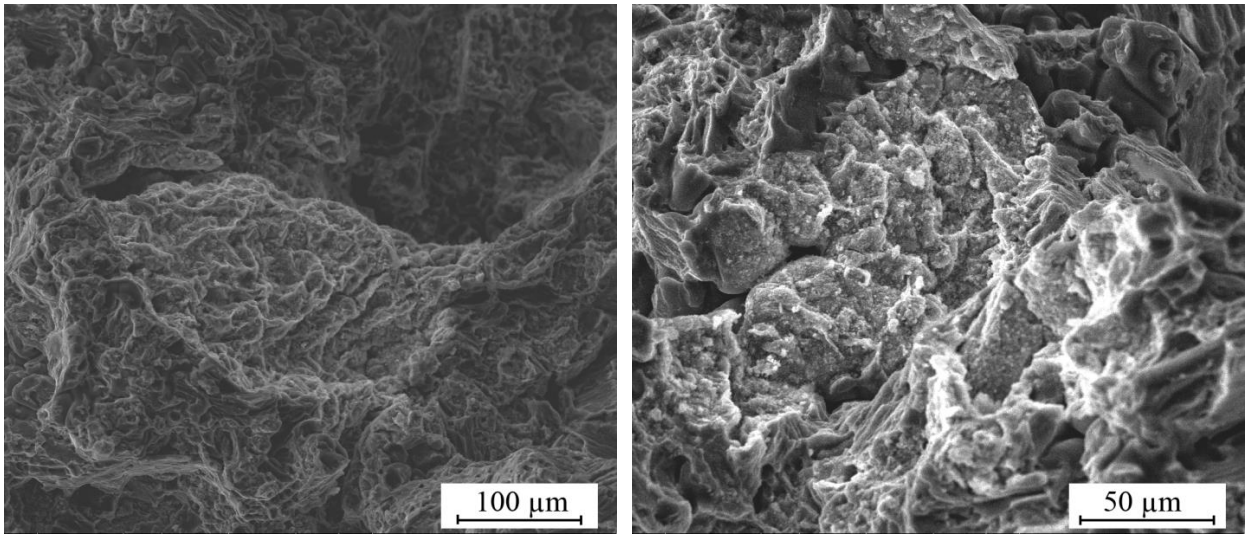

(**a**) (**b**)

Figure 15. Fracture surface of heat-treated ZK51A + 0.5 wt.% AlN (**a**) and ZK51A + 1 wt.% AlN (**b**) alloys.

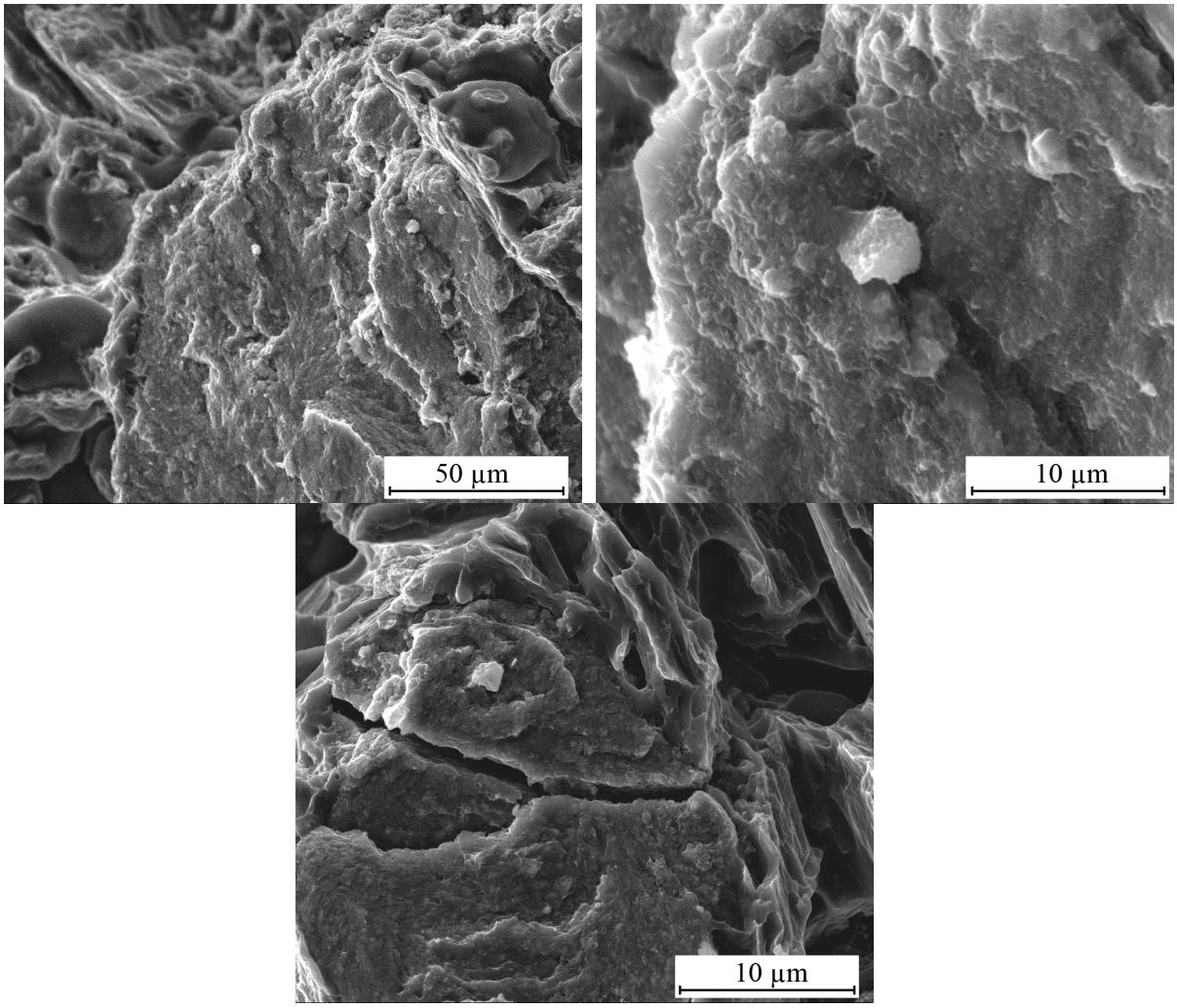

Figure 16. ZnZr phase (light inclusions) in the grain body of ZK51A + 1% AlN alloy after heat treatment.

4. Conclusions

Summing up the results, it can be concluded that the AlN nanoparticle content of 0.5 and 1 wt.% provided the homogeneous grain distribution in Mg alloys having the grain size of 46 and 54 μm, respectively. That was due to the formation of additional solidification centers. At the same time, heat treatment did not affect the grained structure of the alloy.

Heat treatment promotes homogenization of the microstructure of magnesium alloys containing aluminum nitride particles, which reduces the negative influence of undissolved components of the Mg–AlN master alloy.

It was found that the incorporation of 0.1 wt.% AlN resulted in a simultaneous increase in the yield strength (63 to 72 MPa), tensile strength (151 to 212 MPa), and plasticity (6.4 to 19.7%) of the heat-treated alloy due to its dispersion hardening. A further growth in the nanoparticle content led to a reduction in mechanical properties of the alloy because of the formation of agglomerates hampering the attainment of the best mechanical properties. Despite the grain refinement and increase in the mechanical characteristics of the magnesium alloy during tension, its hardness decreases with increasing aluminum nitride content, since the introduction of particles contributes to the formation of additional pore space.

Aluminum nitride particles do not affect the mechanism of destruction of the metal matrix, which is characterized by a lamellar transcrystalline nature of destruction.

Author Contributions: Conceptualization, A.B.V., I.A.Z. and A.P.K.; methodology, A.B.V., I.A.Z., M.V.G. and A.P.K.; investigation, A.A.A., M.V.G. and A.P.K.; writing—original draft preparation, A.A.A. and A.P.K.; writing—review and editing, A.A.A., A.P.K. and I.A.Z.; project administration and funding acquisition, I.A.Z.; and supervision, A.B.V. All authors have read and agreed to the published version of the manuscript.

Funding: This work was carried out with financial support from the Ministry of Education and Science of the Russian Federation (State assignment No. FSWM-2020-0028).

Data Availability Statement: The data presented in this study are available in the article.

Acknowledgments: The research was done using equipment of the Tomsk Regional Core Shared Research Facilities Centre of National Research Tomsk State University.

Conflicts of Interest: The authors declare no conflicts of interest.

References

1. Song, G.L.; Xu, Z.Q. The surface, microstructure and corrosion of magnesium alloy AZ31 sheet. *Electrochim. Acta* **2010**, *55*, 4148–4161. [CrossRef]
2. Morozova, G.I. Phase composition and corrosion resistance of magnesium alloys. *Met. Sci. Heat. Treat.* **2008**, *50*, 100–104. [CrossRef]
3. Jayasathyakawin, S.; Ravichandran, M.; Baskar, N.; Anand Chairman, C.; Balasundaram, R. Mechanical properties and applications of Magnesium alloy–Review. *Mat. Tod. Proc.* **2020**, *27*, 909–913. [CrossRef]
4. Penghuai, F.; Liming, P.; Haiyan, J.; Wenjiang, D.; Chunquan, Z. Tensile properties of high strength cast Mg alloys at room temperature: A review. *China Foundry* **2014**, *11*, 277–286.
5. Ramalingam, V.V.; Ramasamy, P.; Kovukkal, M.D.; Myilsamy, G. Research and Development in Magnesium Alloys for Industrial and Biomedical Applications: A Review. *Met. Mater. Int.* **2020**, *26*, 409–430. [CrossRef]
6. Reinor, G.V. *The Physical Metallurgy of Magnesium and Its Alloys*; Metallurgiya: Moscow, Russia, 1964; 477p. (In Russian)
7. Li, P.; Hou, D.; Han, E.H.; Chen, R.; Shan, Z. Solidification of Mg–Zn–Zr alloys: Grain growth restriction, dendrite coherency and grain size. *Acta Metall. Sin. Engl. Lett.* **2020**, *33*, 1477–1486. [CrossRef]
8. Qian, M.; Das, A. Grain refinement of magnesium alloys by zirconium: Formation of equiaxed grains. *Scr. Mater.* **2006**, *54*, 881–886. [CrossRef]
9. Xing, F.; Guo, F.; Su, J.; Zhao, X.; Cai, H. The existing forms of Zr in Mg-Zn-Zr magnesium alloys and its grain refinement mechanism. *Mater. Res. Express.* **2021**, *8*, 066516. [CrossRef]
10. Song, C.; Han, Q.; Zhai, Q. Review of grain refinement methods for as-cast microstructure of magnesium alloy. *China Foundry* **2009**, *6*, 93–103.
11. Yang, W.; Liu, L.; Zhang, J.; Ji, S.; Fan, Z. Heterogeneous nucleation in Mg–Zr alloy under die casting condition. *Mater. Lett.* **2015**, *160*, 263–267. [CrossRef]
12. Koltygin, A.V.; Bazhenov, V.E.; Letyagin, N.V.; Belov, V.D. The influence of composition and heat treatment on the phase composition and mechanical properties of ML19 magnesium alloy. *Russ. J. Non-Ferr. Met.* **2018**, *59*, 32–41. [CrossRef]

13. Wang, S.; Zhao, Y.; Guo, H.; Lan, F.; Hou, H. Mechanical and Thermal Conductivity Properties of Enhanced Phases in Mg-Zn-Zr System from First Principles. *Materials* **2018**, *11*, 2010. [CrossRef] [PubMed]
14. Koltygin, A.V.; Bazhenov, V.E. Influence of the chemical composition and heat treatment modes on the phase composition and mechanical properties of the ZK51A (ML12) alloy. *Russ. J. Non-Ferr. Met.* **2018**, *59*, 190–199. [CrossRef]
15. Morozova, G.I.; Tikhonova, V.V.; Lashko, N.F. Phase composition and mechanical properties of cast Mg−Zn−Zr alloys. *Met. Sci. Heat. Treat.* **1978**, *20*, 657–660. [CrossRef]
16. Morozova, G.I.; Mukhina, I.Y. Nanostructural hardening of cast magnesium alloys of the Mg–Zn–Zr system. *Met. Sci. Heat. Treat.* **2011**, *53*, 3. [CrossRef]
17. Mukhina, I.Y. Structure and properties of new foundry magnesium alloys. *Foundry Prod.* **2011**, *12*, 12–14. (In Russian)
18. Vorozhtsov, S.A.; Khrustalyov, A.P.; Eskin, D.G.; Kulkov, S.N.; Alba-Baena, N. The physical-mechanical and electrical properties of cast aluminum-based alloys reinforced with diamond nanoparticles. *Russ. Phys. J.* **2015**, *57*, 1485–1490. [CrossRef]
19. Zheng, H.R.; Li, Z.; You, C.; Liu, D.B.; Chen, M.F. Effects of MgO modified β-TCP nanoparticles on the microstructure and properties of β-TCP/Mg-Zn-Zr composites. *Bioactive Mater.* **2017**, *2*, 1–9. [CrossRef]
20. Wong, W.L.; Gupta, M. Effect of hybrid length scales (micro+ nano) of SiC reinforcement on the properties of magnesium. *Solid State Phenom.* **2006**, *111*, 91–94. [CrossRef]
21. Hassan, S.F.; Gupta, M. Creation of high-performance Mg based composite containing nano-size Al_2O_3 particulates as reinforcement. *J. Metast. Nanocr. Mat.* **2005**, *23*, 151–154. [CrossRef]
22. Zhang, B.; Yang, C.; Zhao, D.; Sun, Y.; Wang, X.; Liu, F. Microstructure characteristics and enhanced tensile properties of in-situ AlN/AZ91 composites prepared by liquid nitriding method. *Mater. Sci. Eng. A* **2018**, *725*, 207–214. [CrossRef]
23. Fu, H.M.; Zhang, M.X.; Qiu, D.; Kelly, P.M.; Taylor, J.A. Grain refinement by AlN particles in Mg–Al based alloys. *J. Alloys Compd.* **2009**, *478*, 809–812. [CrossRef]
24. Cao, G.; Choi, H.; Oportus, J.; Konishi, H.; Li, X. Study on tensile properties and microstructure of cast AZ91D/AlN nanocomposites. *Mater. Sci. Eng. A* **2008**, *494*, 127–131. [CrossRef]
25. Berkmortel, R.; Wang, G.G.; Bakke, P. Fluxless in-house recycling of high purity magnesium die cast alloys at Meridian operations. In Proceedings of the 57th IMA Conference, Vancouver BC, Canada, 21–23 May 2000; pp. 22–27.
26. Liu, P.; Geng, H.R.; Wang, Z.Q.; Zhu, J.R.; Pan, F.S.; Dong, X.B. Effect of AlN on Microstructure and Mechanical Properties of Mg-Al-Zn Alloy. *Mater. Sci. Forum* **2011**, *704–705*, 1095–1099. [CrossRef]
27. Wahab, M.N.; Daud, A.R.; Ghazali, M.J. Preparation and characterization of stir cast-aluminum nitride reinforced aluminum metal matrix composites. *Int. J. Mech. Mater. Eng.* **2009**, *4*, 115–117.
28. Vinayagam, M.; Ravichandran, M. Influence of AlN particles on microstructure, mechanical and tribological behaviour in AA6351 aluminum alloy. *Mater. Res. Express* **2019**, *6*, 106557. [CrossRef]
29. Huang, S.J.; Abbas, A. Effects of tungsten disulfide on microstructure and mechanical properties of AZ91 magnesium alloy manufactured by stir casting. *J. Alloys Compd.* **2020**, *817*, 153321. [CrossRef]
30. Hassan, S.F.; Gupta, M. Enhancing physical and mechanical properties of Mg using nanosized Al_2O_3 particulates as reinforcement. *Metall. Mater. Trans. A* **2005**, *36*, 2253–2258. [CrossRef]
31. Sajuri, Z.B.; Miyashita, Y.; Hosokai, Y.; Mutoh, Y. Effects of Mn content and texture on fatigue properties of as-cast and extruded AZ61 magnesium alloys. *Inter. J. Mech. Sci.* **2006**, *48*, 198–209. [CrossRef]
32. Pan, F.; Yang, M.; Chen, X. A review on casting magnesium alloys: Modification of commercial alloys and development of new alloys. *J. Mater. Sci. Tech.* **2016**, *32*, 1211–1221. [CrossRef]
33. Kakhidze, N.I.; Khrustalev, A.P.; Akhmadieva, A.A.; Zhukov, I.A.; Vorozhtsov, A.B. Influence of tungsten nanoparticles on the structure and mechanical behavior of AA5056 under quasi-static loading. In *Light Metals*; Springer: Cham, Switzerland, 2022; pp. 97–103. [CrossRef]
34. Khrustalyov, A.; Kakhidze, N.; Platov, V.; Zhukov, I.; Vorozhtsov, A. Influence of tungsten nanoparticles on microstructure and mechanical properties of an Al-5% mg alloy produced by casting. *Metals* **2022**, *12*, 989. [CrossRef]
35. Khrustalyov, A.P.; Akhmadieva, A.; Monogenov, A.N.; Zhukov, I.A.; Marchenko, E.S.; Vorozhtsov, A.B. Study of the effect of diamond nanoparticles on the structure and mechanical properties of the medical Mg–Ca–Zn magnesium alloy. *Metals* **2022**, *12*, 206. [CrossRef]
36. Lerner, M.; Vorozhtsov, A.; Guseinov, S.; Storozhenko, P. *Metal Nanopowders: Production Characterization, and Energetic Applications*; Wiley-VCH: Weinheim, Germany, 2014; pp. 79–106.
37. Khrustalyov, A.; Zhukov, I.; Nikitin, P.; Kolarik, V.; Klein, F.; Akhmadieva, A.; Vorozhtsov, A. Study of Influence of aluminum nitride nanoparticles on the structure, phase composition and mechanical properties of AZ91 alloy. *Metals* **2022**, *12*, 277. [CrossRef]
38. Orlov, D.; Pelliccia, D.; Fang, X.; Bourgeois, L.; Kirby, N.; Nikulin, A.Y.; Ameyama, K.; Estrin, Y. Particle evolution in Mg–Zn–Zr alloy processed by integrated extrusion and equal channel angular pressing: Evaluation by electron microscopy and synchrotron small-angle X-ray scattering. *Acta Mater.* **2014**, *72*, 110–124. [CrossRef]
39. Liu, S.; Yang, W.; Shi, X.; Li, B.; Duan, S.; Guo, H.; Guo, J. Influence of laser process parameters on the densification, microstructure, and mechanical properties of a selective laser melted AZ61 magnesium alloy. *J. Alloys Compd.* **2019**, *808*, 151160. [CrossRef]
40. Wang, B.J.; Xu, D.K.; Sun, J.; Han, E.H. Effect of grain structure on the stress corrosion cracking (SCC) behavior of an as-extruded Mg-Zn-Zr alloy. *Corr. Sci.* **2019**, *157*, 347–356. [CrossRef]

41. Dieringa, H.; Katsarou, L.; Buzolin, R.; Szakács, G.; Horstmann, M.; Wolff, M.; Mendis, C.; Vorozhtsov, S.; StJohn, D. Ultrasound Assisted Casting of an AM60 Based Metal Matrix Nanocomposite, Its Properties, and Recyclability. *Metals* **2017**, *7*, 388. [CrossRef]
42. Khrustalyov, A.P.; Garkushin, G.V.; Zhukov, I.A.; Razorenov, S.V.; Vorozhtsov, A.B. Quasi-Static and Plate Impact Loading of Cast Magnesium Alloy ML5 Reinforced with Aluminum Nitride Nanoparticles. *Metals* **2019**, *9*, 715. [CrossRef]
43. Petch, N. The cleavage strength of polycrystals. *J. Iron Steel Inst.* **1953**, *174*, 25–28.